Eur. Phys. J. D **23**, 35–42 (2003)
DOI: 10.1140/epjd/e2003-00021-1

THE EUROPEAN PHYSICAL JOURNAL D

Investigation of auto-ionizing states in xenon by resonantly enhanced multi-photon ionization

M. Stellpflug, M. Johnsson, I.D. Petrov[a], and T. Halfmann[b]

Fachbereich Physik der Universität, 67653 Kaiserslautern, Germany

Received 30 September 2002
Published online 28 January 2003 –

Abstract. We have examined the autoionization spectrum of xenon by resonantly enhanced three-photon ionization ($2+1$ REMPI) involving intermediate states $5p^5 6p\,[J=0,2]$. The properties of the observed autoionization resonances change significantly with the choice of the intermediate state. For ionization *via* an intermediate state with predominantly $5p^5(^2\mathrm{P}_{3/2})$ core character, a strong continuum with embedded window-type $5p^5(^2\mathrm{P}_{1/2})\,nd'$-autoionization resonances is observed. For intermediate states, predominantly with $5p^5(^2\mathrm{P}_{1/2})$ core character, both $5p^5(^2\mathrm{P}_{1/2})\,nd'$- as well as $5p^5(^2\mathrm{P}_{1/2})\,ns'$-resonances are present in the spectrum as overlapping, nearly symmetric peaks on a rather weak continuum. Calculations confirm the significant dependence of the spectral lineshapes upon the excitation pathway to the autoionizing state. The ionization data are compared with spectra obtained by monitoring third-harmonic generation *via* autoionizing states without resonant excitation of intermediate states. These spectra also exhibit the signature of both the nd'- and ns'-resonances.

PACS. 32.80.Dz Autoionization

1 Introduction

The highly excited and autoionizing states of heavy rare gases permit the preparation of population in energy levels well above 10 eV. Thus they have attracted much attention in many fields of current scientific interest. Among applications we note *e.g.* nonlinear optics with rare gases providing efficient sources for the generation of short-wavelength (vacuum-ultraviolet) radiation [8–10]. The properties (*i.e.* the lineshape) of autoionizing resonances play a crucial role in processes involving such states [11].

Autoionization lineshapes, which in general can exhibit both enhancement as well as suppression of ionization, are described by the profile parameter q [13]. This parameter depends strongly upon the choice of the excitation pathway from an initial state, usually *via* intermediate states, to the excited state (see, *e.g.* [3]).

In contrast to investigations on autoionization lineshapes in heavy rare gases based on single-photon excitation from the ground state by vacuum-ultraviolet radiation [1,2] or starting from otherwise excited metastable states [5], resonantly enhanced multi-colour and multi-photon couplings [4] permit a broader variation of excitation pathways and can be implemented with radiation of moderate photon energy in the ultraviolet and visible spectral range. By tuning the exciting laser pulses to different intermediate states, the effect of different excitation pathways on the autoionization lineshape can be investigated.

In this work we show, how the lineshapes of autoionizing resonances in xenon are dramatically modified, if pathways starting from the ground state *via* different intermediate states, belonging to different core configurations, are excited. This leads to a significant variation of the autoionization spectrum, *e.g.* in enhanced or suppressed, even apparently missing resonances. We compare our results, obtained from resonantly enhanced three-photon ionization with data from third-harmonic generation and with calculations, based on the configuration interaction Pauli-Fock method including core polarization [20].

2 Atomic coupling scheme

The ionization continuum of xenon, as in any other heavy rare gas atom, possesses a double structure, belonging to the two fine structure components of the xenon ion $\mathrm{Xe}^+\ ^2\mathrm{P}_{3/2}$ and $\mathrm{Xe}^+\ ^2\mathrm{P}_{1/2}$. Thus, the bound states of xenon consist of two series of states, converging either to the threshold of the $\mathrm{Xe}^+\ ^2\mathrm{P}_{3/2}$ or the $\mathrm{Xe}^+\ ^2\mathrm{P}_{1/2}$ continuum. The states converging to the higher threshold $\mathrm{Xe}^+\ ^2\mathrm{P}_{1/2}$ are energetically degenerate with the lower continuum and

[a] *Permanent address*: Rostov State University of Transport Communication, 344038, Rostov-on-Don, Russia.
[b] e-mail: halfmann@physik.uni-kl.de

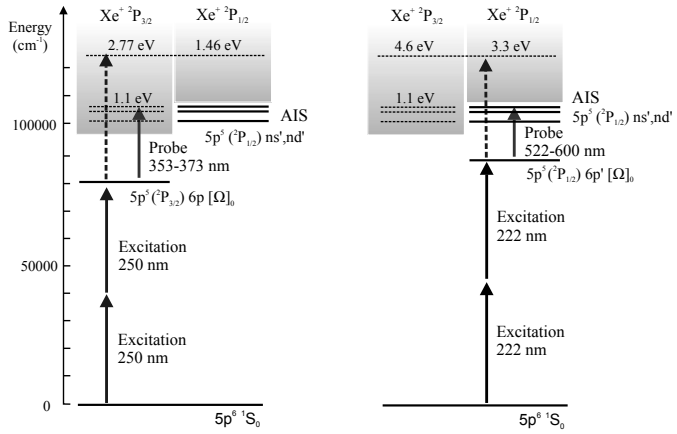

Fig. 1. Coupling schemes for two-colour resonantly enhanced three-photon ionization of xenon *via* intermediate states with different core configurations $^2\mathrm{P}_{3/2}$ (l.h.s., state $5p^5(^2\mathrm{P}_{3/2})6p[1/2]_0$) or $^2\mathrm{P}_{1/2}$ (r.h.s., state $5p^5(^2\mathrm{P}_{1/2})6p'[1/2]_0$). Alternatively state $5p^5(^2\mathrm{P}_{1/2})6p'[3/2]_2$, also belonging to core configuration $^2\mathrm{P}_{1/2}$ was excited (excitation laser wavelength 224 nm; for reasons of clarity this path is not plotted in the figure). The excitation laser pulse drives population from the ground state $5p^6\ ^1\mathrm{S}_0$ to the intermediate state *via* a two-photon transition. Some population of the intermediate state is ionized by absorbing a third photon from the excitation laser, generating photoelectrons with higher kinetic energy. A probe laser, time delayed with respect to the excitation laser, couples the intermediate state to autoionizing states (AIS). The autoionization spectrum is monitored by detection of the photoelectrons with lower kinetic energy.

experience strong autoionization [14] (see Fig. 1). To emphasize the properties of a bound state in xenon with respect to the continuum it belongs to, we add the quantum number of the ionic core in our spectroscopic notation, following the nomenclature used in standard literature [25].

Figure 1 shows the relevant coupling schemes for the experiments discussed here. The atomic ground state $5p^6\ ^1\mathrm{S}_0$ is coupled by an excitation laser pulse, inducing a two-photon transition to an intermediate state, either $5p^5(^2\mathrm{P}_{3/2})6p[1/2]_0$ or $5p^5(^2\mathrm{P}_{1/2})6p'[1/2]_0$. A probe laser pulse couples the intermediate state to autoionizing states with quantum numbers $5p^5(^2\mathrm{P}_{1/2})ns'\,[J=1]$ or $5p^5(^2\mathrm{P}_{1/2})nd'\,[J=1]$. In the spectral range of our investigations the principal quantum number was $n \geq 11$. The probe laser pulse was delayed with respect to the pump laser. For the case of coincident laser pulses, competing interactions, *e.g.* coherent population trapping [16–18] could perturb the system and interfere with the autoionization process.

With the probe laser tuned in the range of the autoionizing states, the spectral lineshape of autoionization resonances was recorded by monitoring the photoelelectrons generated in the lower continuum following autoionization. Unlike *e.g.* metastable xenon $5p^5(^2\mathrm{P}_{1/2})6s\,[J=0]$, which is strongly mixed with the nearby state $5p^5(^2\mathrm{P}_{3/2})5d\,[J=0]$ [7], the states $5p^5(^2\mathrm{P}_{3/2})6p[1/2]_0$ and $5p^5(^2\mathrm{P}_{1/2})6p'[1/2]_0$ do not show significant admixture of neighbouring states.

Autoionization is described by Fano's theory [13] considering the excitation from a (bound) initial state $|1\rangle$ to a (bound) excited state $|2\rangle$ degenerate with a (*e.g.* ionization) continuum state $|C,E\rangle$ with energy E. This interaction leads to a new state [13] which is a mixture of the bound and the continuum state, *i.e.* an autoionization resonance. The photoionization cross-section reads in the form of a generalized Beutler-Fano profile, including summation over N autoionization resonances [13,15]

$$\sigma = \sum_i^N \sigma_0 \rho_i^2 \left[\frac{(q_i+\epsilon_i)^2}{1+\epsilon_i^2} - 1\right] + \sigma_0, \tag{1}$$

where σ_0 is the ionization cross-section in the non-resonant region, ρ^2 describes the ratio of ionization on resonance with respect to non-resonant ionization, q is the profile parameter and ϵ is a dimensionless energy,

$$\epsilon = (E - E_R)/(\Gamma/2) \tag{2}$$

including the resonance energy E_R and the linewidth Γ. The profile parameter q is given by [12,13]

$$q = \frac{\langle 1|\mu|2\rangle + P\int \mathrm{d}E' \langle 1|\mu|C,E'\rangle\langle C,E'|T|2\rangle/(E_R-E')}{\pi\langle 1|\mu|C,E_R\rangle\langle C,E_R|T|2\rangle} \tag{3}$$

where μ is the electric dipole operator, T is the operator (electron-electron interaction) which couples state $|2\rangle$ to the continuum, and P indicates the principal part of the following integral. Equation (3) suggests, that the choice of the initial state $|1\rangle$ strongly determines the profile parameter q and thus the shape of the autoionization resonance, as first confirmed experimentally by Ganz *et al.* [3].

3 Experimental setup

A supersonic jet of rare gas atoms in natural abundance was expanded from a stagnation region at room temperature and a pressure of typically 500 mbar through a pulsed nozzle (General Valve, opening diameter 0.8 mm). The resulting jet was collimated by a skimmer (orifice 0.8 mm), 132 mm downstream of the nozzle. The skimmer separated the source chamber from the interaction and detection region. The pulsed beam of rare gas atoms was intersected by the lasers at right angle at a distance of 103 mm downstream from the skimmer. The particle density in the interaction region is estimated to be approximately 10^{13} atoms/cm^3.

The laser pulses were generated in two pulsed dye lasers (Lambda Physics LPD 3000), synchronously pumped by an excimer laser (Lambda Physics LPX 220), operating at 308 nm with a repetition rate of typically several 10 Hz. The laser pulses had a bandwidth of 6 GHz and a pulse duration of approximately 15 ns. The output of the first dye laser was frequency doubled in a BBO crystal to generate ultraviolet radiation

at 250 nm, 222 nm or 224 nm, which served to excite population *via* a two-photon transition from the atomic ground state $5p^6\ {}^1S_0$ of xenon to either of the intermediate states $5p^5({}^2P_{3/2})6p[1/2]_0$, $5p^5({}^2P_{1/2})6p'[1/2]_0$ or $5p^5({}^2P_{1/2})6p'[3/2]_2$. Absorption of a third photon from the same radiation field limited the population of the intermediate state by the competing process of resonantly enhanced three-photon ionization. The output of the second dye laser passed an optical delay line to be separated from the excitation pulse by up to 40 ns. The probe laser pulse was used to excite transitions from the intermediate state to an autoionizing state $5p^5({}^2P_{1/2})\,ns'$ or $5p^5({}^2P_{1/2})\,nd'$, decaying to the $^2P_{3/2}$ continuum. For the spectra belonging to the intermediate state $5p^5({}^2P_{3/2})6p[1/2]_0$ the output of the probe laser was frequency doubled in a BBO crystal, while for the spectra belonging to the other intermediate states the visible radiation of the laser was used directly. The pulse energy of the visible radiation was typically several mJ, while several 100 μJ were obtained in the second harmonic frequency of the dye laser.

The laser pulses were spatially overlapped and focussed with quartz lenses (f = 300 mm) into the interaction region. The diameter of the exciting laser pulse in the interaction region was approximately 150 μm (FWHM), while the diameter of the ionizing laser pulse was kept in the range of typically 0.5 mm (FWHM). This setup yielded maximum laser intensities up to several 100 MW/cm^2 for the excitation laser and typically 10–100 MW/cm^2 for the ionizing laser. At this intensity the autoionization resonances exhibited strong power broadening (see below).

As discussed above both lasers contributed to the total ionization signal. Therefore an electron spectrometer was used in order to separate the photoelectrons belonging to the different channels, *i.e.* resonantly enhanced three-photon ionization to both continua by the excitation laser and autoionization to the $^2P_{3/2}$ continuum induced by the probe laser.

We used an electron spectrometer, based on an electrostatic parabolic mirror, which is described in detail in previous publications [18,19]. Briefly the setup is as follows: the field-free interaction region of the electron spectrometer was located in the focus of an electrostatic parabolic mirror. After ionization the generated photoelectrons left the field-free region, were accelerated and traveled along a time-of-flight segment at the end of which they were detected on a micro-sphere plate (El Mul Technologies). The signal output of the micro-sphere plate was amplified by fast broadband amplifiers and processed in boxcar gated integrators (EG&G 4121B). The energy resolution of the spectrometer was typically 150 meV at $E_{\rm kin}$ = 4 eV, which was sufficient to resolve photoelectrons generated in the different processes.

A second experimental setup was used to monitor third-harmonic generation *via* autoionizing states (see Fig. 5), which was compared to the spectra obtained from two-colour resonantly enhanced three-photon ionization,

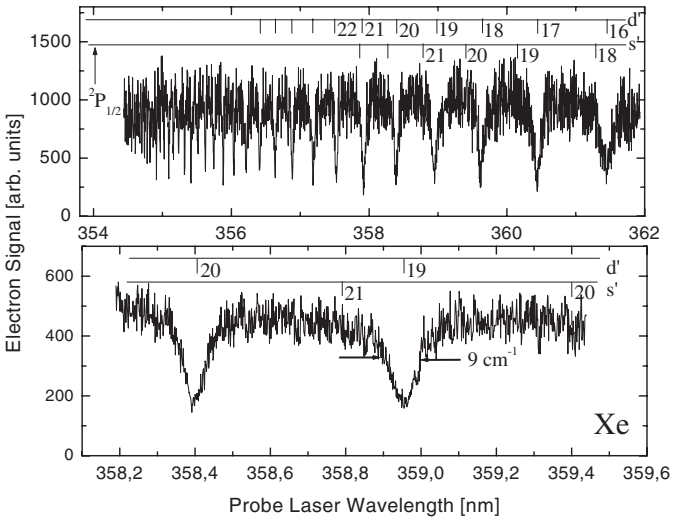

Fig. 2. Two-colour resonantly enhanced three-photon ionization in xenon *via* an intermediate state with core configuration $^2P_{3/2}$. The frequency of the excitation laser was fixed to the transition from the ground to the intermediate state $5p^5({}^2P_{3/2})6p[1/2]_0$, while the frequency of the probe laser was tuned in the range of the autoionizing states. The spectrum exhibits only window-type nd'-resonances, while no contributions from ns'-states are visible. The linewidth of the $19d'$-resonance is close, but not equal to the expected experimental value of 6.9 cm^{-1} (see *e.g.* Ref. [27]), thus indicating some contribution due to powerbroadening.

described above. The setup for third-harmonic generation was as follows.

The frequency doubled output of a single excimer-laser pumped dye laser (see above), pulse energy up to 1 mJ at 280 nm, was focussed with a quartz lens (f = 180 mm) into an atomic jet, yielding intensities up to the regime of several GW/cm^2. The supersonic jet of xenon atoms in natural abundance was generated by a pulsed nozzle (General Valve, opening diameter 0.8 mm). The focussed laser beam intersected the atomic beam right behind the nozzle orifice, at a distance of typically less than 1 mm. The particle density in the interaction region is estimated to be approximately 10^{19} atoms/cm^3.

Vacuum-ultraviolet radiation around 93 nm, *i.e.* the third-harmonic frequency of the driving laser pulse was generated by nonlinear optical interaction with the xenon atoms. The copropagating fundamental and third harmonic frequency entered a vacuum spectrometer (Acton Research VM502), equipped with a grating (1 200 lines/mm) to separate the vacuum-ultraviolet radiation from the fundamental frequency and direct it onto an electron multiplier tube (Hamamatsu, type R595). The signal output of the electron multipler was amplified and processed the same way as described above.

4 Experimental results

Figure 2 shows the photoelectron signal from the autoionizing states in xenon with the frequency of the probe laser

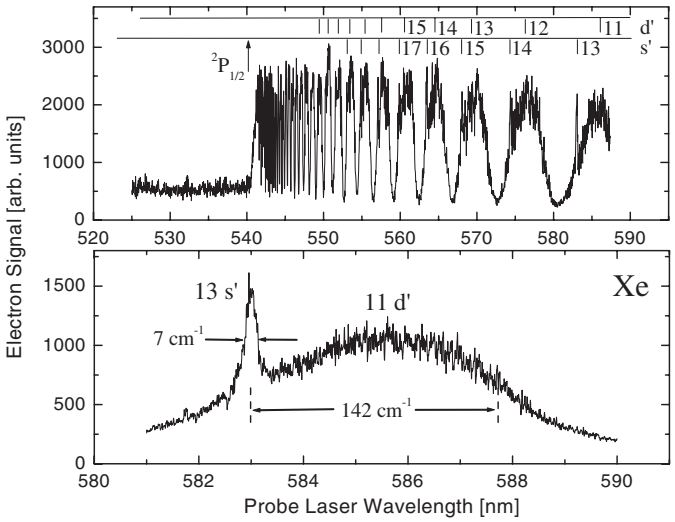

Fig. 3. Two-colour resonantly enhanced three-photon ionization in xenon *via* an intermediate state with core configuration $^2P_{1/2}$. The frequency of the excitation laser was fixed to the transition from the ground to the intermediate state $5p^5(^2P_{1/2})6p'[1/2]_0$, while the frequency of the probe laser was tuned in the range of the autoionizing states. Both the nd'- as well as the ns'-resonances are clearly visible in the spectrum. The resonances exhibit strong powerbroadening, as comparison with theory shows. The expected linewidth of the $13s'$-resonance is 1.2 cm^{-1} (see Ref. [27]). that of the $11d'$-resonance is 49 cm^{-1} (see Ref. [27]). These values are well below the observed, powerbroadened linewidths, indicated in the spectrum.

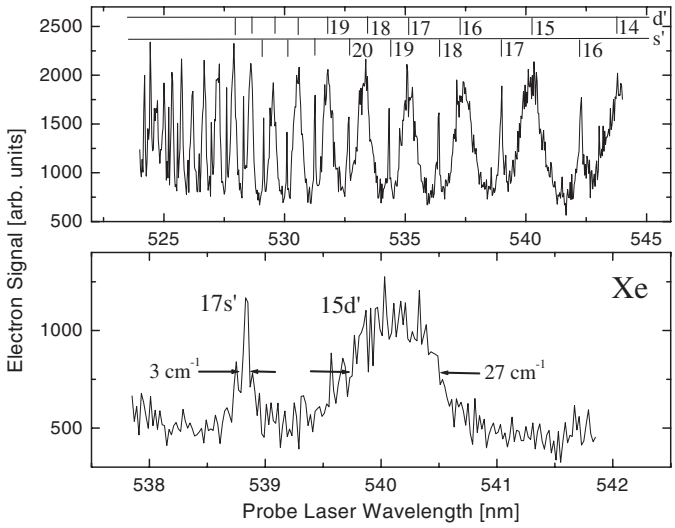

Fig. 4. Two-colour resonantly enhanced three-photon ionization in xenon *via* the intermediate state $5p^5(^2P_{1/2})6p'[3/2]_2$, belonging to core configuration $^2P_{1/2}$. The frequency of the excitation laser was fixed to the transition from the ground to the intermediate state $5p^5(^2P_{1/2})6p'[3/2]_2$, while the frequency of the probe laser was tuned in the range of the autoionizing states. As in the case of the intermediate state $5p^5(^2P_{1/2})6p'[1/2]_0$ (see Fig. 3) the ns' resonances are visible besides nd' resonances. Due to the smaller linewidth of the nd' resonances the resolution of the autoionizing ns' states is better than in Figure 3. The resonances exhibit strong powerbroadening. The expected linewidth of the $17s'$-resonance is only 0.4 cm^{-1} (see Ref. [27]). The effective linewidth of the $15d'$-resonance depends on the composition of the excited $[K']_J$ components. In view of the resonance shape (compare to Fig. 3), excitation of the $nd'(J = 1)$- resonance appears to be weak. The $nd'(J = 2, 3)$-resonances have expected linewidths between 6.1 cm^{-1} and 1.1 cm^{-1} (see Ref. [27]), much lower than the effective linewidth of the observed nd'-resonance.

varied and the frequency of the exciting laser pulse tuned to the two-photon resonance between the ground state $5p^6\ ^1S_0$ and the intermediate state $5p^5(^2P_{3/2})6p[1/2]_0$.

The spectrum exhibits the progression of window-type nd'-resonances, *i.e.* only ionization suppression, but no enhancement is observed on resonance. Thus the profile parameter q is close to zero. Besides the nd'-progression ns'-resonances are *not* visible in the spectrum.

In contrast, when the frequency of the exciting laser was tuned to two-photon resonance with the intermediate state $5p^5(^2P_{1/2})6p'[1/2]_0$, the autoionization spectrum clearly shows both the nd'- as well as the ns'-resonances (see Fig. 3). As it is well known, the linewidth of the ns'-resonances is small compared to that of the nd'-resonances [1,2]. The absolute value of the profile parameter for both progressions is much larger than unity, *i.e.* the ionization enhancement on resonance is large with respect to the non-resonant background. For the nd'-resonances q is obviously negative, *i.e.* the ionization enhancement occurs at longer wavelength, while the ionization dip is observed at shorter wavelength. In comparison to data obtained by one-photon excitation of autoionizing states with vacuum-ultraviolet radiation [2] the sign of the profile parameter is reversed in the excitation pathway chosen here.

When the exciting laser is tuned to the intermediate state $5p^5(^2P_{1/2})6p'[3/2]_2$, the nd'-resonances with $J = 2, 3$ are predominately excited, and thus are expected to have smaller linewidth than the $nd'\,[J = 1]$ series [27]. This permits clearer separation of the $ns'\,[J = 1]$-resonances (see Fig. 4). As in the case of the intermediate state $5p^5(^2P_{1/2})6p'[1/2]_0$ the profile parameter q is large both for the nd'- as well as the ns'-resonances.

The autoionization spectra in Figures 3 and 4 exhibit strong powerbroadening, as concluded from the known width of these resonances [27].

While the spectra discussed above involved *resonant* excitation of different intermediate states, we compared these data with three-photon excitation, *off-resonant* with any possible intermediate state. Because our setup to detect photoionization products was not sensitive enough to observe such off-resonant three-photon ionization, we monitored third-harmonic generation *via* autoionizing states instead (see Fig. 5). Figure 6 shows the signal from third-harmonic generation when the frequency of a single laser pulse was tuned in the range of the autoionization resonances. Both the nd'-resonances as well as the ns'-resonances are clearly visible. The sign of the profile parameters for both progressions is negative. The lineshapes of the resonances obtained in third-harmonic generation differ from those recorded by photoionization detection [2]

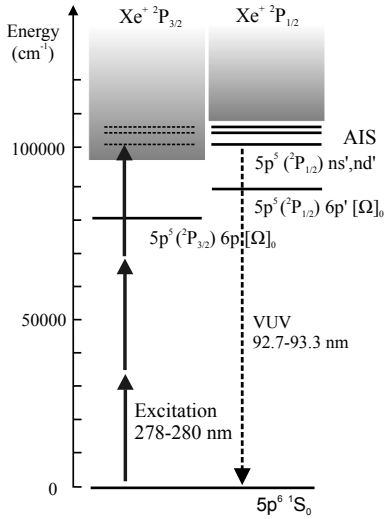

Fig. 5. Coupling scheme for third-harmonic generation *via* autoionizing states in xenon. The frequency of a single (excitation) laser pulse is tuned to three-photon resonance with autoionizing states. The nonlinear susceptibility of the medium drives generation of vacuum-ultraviolet (VUV) radiation.

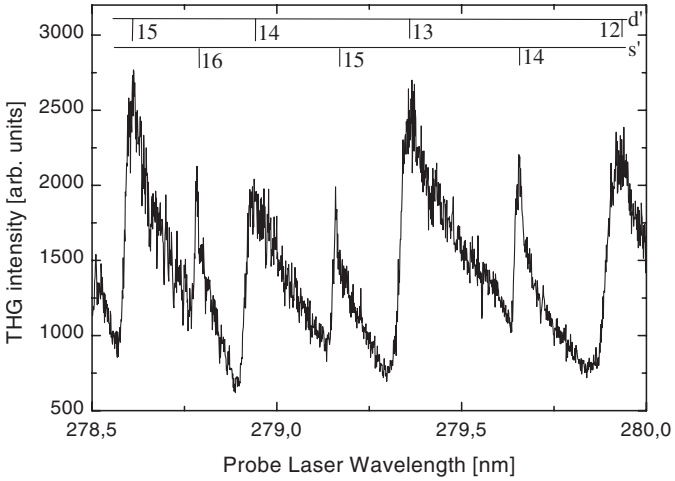

Fig. 6. Third-harmonic generation *via* autoionizing states in xenon. When the frequency of the excitation laser is tuned in the vicinity of three-photon resonance with an autoionizing state, the third-harmonic yield is significantly modulated. Both the nd'- as well as the ns'-resonances are clearly visible in the spectrum. In contrast to the spectra monitored by resonantly enhanced three-photon ionization (see Figs. 2, 3, 4) there are no resonantly excited intermediate states involved in the frequency conversion process.

which we attribute mainly to the manifold of virtual intermediate states involving contributions to the off-resonant third-order (nonlinear) optical process [11]. In addition the frequency conversion process competes with population depletion resp. photoionization and reabsorption processes, as it is well-known for third-harmonic generation in the vicinity of excited states [6]. Therefore a detailed analysis of the lineshapes obtained in third-harmonic generation is not as straightforward as in the case of the spectra monitored by photoionization.

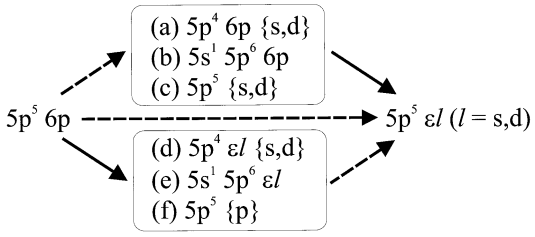

Fig. 7. Correlation diagram for photoionization of state $5p^5\,6p$. Dashed lines denote electric dipole interaction, solid lines indicate Coulomb interaction.

We like to note, that we also examined autoionization spectra in krypton, involving intermediate states belonging to the different core configurations $Kr^+\,^2P_{1/2}$ and $Kr^+\,^2P_{3/2}$. These spectra show similar behaviour as the xenon spectra discussed here.

5 Discussion and theoretical calculations

The data presented in the previous section clearly demonstrate the significant variation of autoionization spectra upon the choice of the excitation pathway. While the ns'-resonances are clearly visible in spectra involving resonant excitation *via* intermediate states belonging to the core configuration $^2P_{1/2}$ (see Figs. 3 and 4), they seem to vanish in the spectrum involving an intermediate state with core configuration $^2P_{3/2}$ (see Fig. 2). The autoionization spectra monitored by third-harmonic generation (see Fig. 6) support this observation. Due to the off-resonant character of the excitation, *i.e. via* a *virtual* intermediate state, including couplings to states of *both* core configurations, especially contributions from intermediate states with core configuration $^2P_{1/2}$, the ns'-resonances are clearly visible besides the nd'-resonances.

To understand the experimental data in detail, we have theoretically analyzed the lineshapes of the autoionization resonances.

Photoionization cross-sections of the states $5p^5(^2P_{3/2})6p[1/2]_0$ and $5p^5(^2P_{1/2})6p'[1/2]_0$ in the energy region of the autoionization resonances were calculated in the configuration interaction Pauli-Fock approximation including core polarization (CIPF CP) [20]. The correlations we consider are schematically presented in Figure 7.

In this scheme the upper and lower pathways represent corrections to the amplitudes of the direct transitions $5p^56p \rightarrow 5p^5(^2P_{3/2})\varepsilon l$ resp. $5p^56p \rightarrow 5p^5(^2P_{1/2})nl'$ (with $l, l' = 0, 2$) due to final state configuration interaction (FISCI) and initial state configuration interaction (ISCI), respectively. Here $\{l\}$ denotes the complete set of atomic orbitals (AO) over which summation and integration is performed. The dashed and solid lines denote the electric dipole and Coulomb interaction, respectively. This scheme was computed within second order perturbation

theory (PT). In addition, the next order of PT was partially accounted for by taking the correction Figure 7c to the dipole transition amplitude in a form which includes all electron correlations (Figs. 7a–7f) into account. The influence of high lying configurations was also taken into account as a correlational decrease of the Coulomb interaction by a factor of 1.26 [21].

In the calculation of the radial integrals, entering the expressions for the direct and correlational amplitudes, we used wave functions with a relaxed $5p^5$-core. They were calculated in the Pauli-Fock (PF) approximation [21] which accounts for the relativistic compression of the core orbitals. The s- and d-orbitals of the final and intermediate states in the correlation contribution Figure 7c were calculated in the potential for the $5p^5(^2\mathrm{P}_{1/2})\varepsilon s[1/2]_1$ and $5p^5(^2\mathrm{P}_{1/2})\varepsilon d[3/2]_1$ states, respectively. $\{s, d\}$ orbitals entering the correlations Figures 7a and 7d were obtained in the averaged potential for the configuration $5p^4 6p$ and $5p^4$, respectively. The $6p$-orbital of both initial states was calculated using the electrostatic potential of the $5p^5(^2\mathrm{P}_{1/2})6p'[1/2]_0$ state with orthogonalization to the $5p$-AO. The same potential was used in the calculation of Figure 7f correlation. To avoid problems connected with the calculation of the divergent dipole matrix elements the correlation function technique [22] has been applied.

We like to note a problem arising for the states $5p^5 6p$ with angular momentum $J = 0$. As addressed in [23], the states involved in the dipole transition amplitude must be orthogonalized to the lower energy states with the same symmetry, here the ground state $5p^6\ ^1\mathrm{S}_0$. In the present calculation the problem is solved by setting up the $5p^6$-configuration using the wave functions taken from $5p^5$ configuration and including it in the secular equation matrix for the initial state. The procedure is similar to the technique described in [24].

The spin-orbit coupling constant calculated within the PF approximation for the configuration $5p^5$ was $\zeta_{5p} = 0.785$ eV, but in the present work the experimental spin-orbital parameter $\zeta_{5p} = 0.871$ eV [25] was used to calculate both the elements of the secular matrix and the energies of the $5p^5(^2\mathrm{P}_{1/2})$ and $5p^5(^2\mathrm{P}_{3/2})$ thresholds. The eigenvectors of the secular equation matrix expressed as

$$|5p^5(^2\mathrm{P}_{3/2})6p[1/2]_0\rangle = 0.0910|5p^6\ ^1\mathrm{S}_0\rangle + 0.7666|5p^5 6p\ ^1\mathrm{S}_0\rangle - 0.6356|5p^5 6p\ ^3\mathrm{P}_0\rangle \quad (4)$$

$$|5p^5(^2\mathrm{P}_{1/2})6p'[1/2]_0\rangle = 0.0662|5p^6\ ^1\mathrm{S}_0\rangle + 0.6322|5p^5 6p\ ^1\mathrm{S}_0\rangle + 0.7720|5p^5 6p\ ^3\mathrm{P}_0\rangle \quad (5)$$

were then used as initial states. The energies of these states relative to the $5p^5(^2\mathrm{P}_{3/2})$ threshold were taken from experimental data [25] as $E(5p^5(^2\mathrm{P}_{3/2})6p[1/2]_0) = -2.196$ eV and $E(5p^5(^2\mathrm{P}_{1/2})6p'[1/2]_0) = -0.989$ eV. These were used in the expression for the photoionization cross-section and the energy denominator in the correlation Figure 7f. The theory developed in [26] was applied to take the interaction of the $5p^5(^2\mathrm{P}_{1/2})20s'[1/2]_1$ and $5p^5(^2\mathrm{P}_{1/2})18d'[3/2]_1$ states *via* the $5p^5(^2\mathrm{P}_{3/2})\varepsilon l$ continuum into account. The calculated photoionization cross-sections in the region of the $18d'$- and $20s'$-resonances are presented in Figure 8. The resonances show up as clear peaks on top of a rather weak continuum when excited from the $5p^5(^2\mathrm{P}_{1/2})6p'[1/2]_0$ state, and as windows in a strong continuum when excited from the $5p^5(^2\mathrm{P}_{3/2})6p[1/2]_0$ state. The resonances displayed in Figure 8 can be described as a summation over Beutler-Fano profiles (see Eq. (1)). The resonance parameters ρ_i^2 and q_i entering equation (1) were determined by a fitting procedure to the theoretical cross-section curve whereas E_i, Γ_i and σ_0 were calculated. The parameters are presented in Table 1.

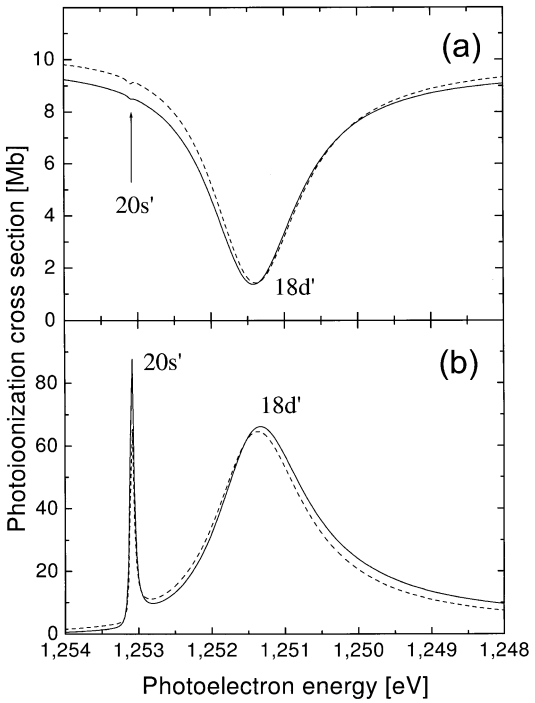

Fig. 8. Photoionization cross-sections of state $5p^5(^2\mathrm{P}_{3/2})6p[1/2]_0$ (upper trace) and $5p^5(^2\mathrm{P}_{1/2})6p'[1/2]_0$ (lower trace) in the vicinity of the autoionization resonances $18d'$ and $20s'$, calculated in the CIPF CP approximation in length form (solid line) and velocity form (dashed line) of the electric dipole operator. Ionization from state $5p^5(^2\mathrm{P}_{3/2})6p[1/2]_0$ yields a dominant window-type $18d'$-resonance with a very weak contribution from the $20s'$-resonance, while the cross-section from state $5p^5(^2\mathrm{P}_{1/2})6p'[1/2]_0$ clearly exhibits both the $18d'$- as well as the $20s'$-autoionization resonance. The energy scale runs from large to small values in order to permit comparison with the experimental data shown in Figures 2 and 3.

In the case of the initial state $5p^5(^2\mathrm{P}_{1/2})6p'[1/2]_0$ the $20s'$ and $18d'$ resonances are both present in the photoionization cross-section as clear peaks (*i.e.* $|q| \gg 1$, see Fig. 8a), whereas in the case of the initial state $5p^5(^2\mathrm{P}_{3/2})6p[1/2]_0$ the autoionizing state $18d'$ exhibits a window resonance (*i.e.* $|q| \approx 0$), while the $20s'$-resonance is almost not visible (see Fig. 8b). The direct amplitudes for the

Table 1. Theoretical parameters of the $5p^5(^2P_{1/2})20s'[1/2]_1$ and $5p^5(^2P_{1/2})18d'[3/2]_1$ resonances. E_i is the predicted photoelectron energy. Velocity form results are given in brackets.

Initial states	Resonance	E_i [eV]	Γ_i [cm^{-1}]	σ_0 [Mb]	q_i	ρ_i^2
$5p^5(^2P_{3/2})6p[1/2]_0$	$5p^5(^2P_{1/2})20s'[1/2]_1$	1.2531	0.478	9.62(10.02)	0.022(−0.191)	0.0107(0.0146)
$5p^5(^2P_{3/2})6p[1/2]_0$	$5p^5(^2P_{1/2})18d'[3/2]_1$	1.2515	11.79	9.62(10.02)	0.058(0.094)	0.851(0.860)
$5p^5(^2P_{1/2})6p'[1/2]_0$	$5p^5(^2P_{1/2})20s'[1/2]_1$	1.2531	0.478	2.32(1.49)	−9.1(−6.9)	0.434(0.874)
$5p^5(^2P_{1/2})6p'[1/2]_0$	$5p^5(^2P_{1/2})18d'[3/2]_1$	1.2515	11.79	2.32(1.49)	−5.6(−7.7)	0.875(0.717)

transitions $5p^5(^2P_{1/2})6p'[1/2]_0 \rightarrow 5p^5(^2P_{1/2})20s'[1/2]_1$ and $5p^5(^2P_{1/2})6p'[1/2]_0 \rightarrow 5p^5(^2P_{1/2})18d'[3/2]_1$ are more than one order of magnitude larger than for the transitions $5p^5(^2P_{3/2})6p[1/2]_0 \rightarrow 5p^5(^2P_{1/2})20s'[1/2]_1$ and $5p^5(^2P_{3/2})6p[1/2]_0 \rightarrow 5p^5(^2P_{1/2})18d'[3/2]_1$ due to the change of the total angular momentum of the $5p$-shell during the transition. However, the imaginary part of the correlational amplitude Figure 7c for the latter transition is large. As a consequence, the $18d'$ resonance appears as a prominent window-type resonance on the background of the $5p^5(^2P_{3/2})6p[1/2]_0 \rightarrow 5p^5(^2P_{3/2})\varepsilon l$ photoionization continuum.

6 Conclusions

We have investigated the lineshapes of autoionization resonances in xenon atoms for multi-photon excitation pathways from the ground state *via* different intermediate states. The autoionization spectrum, *i.e.* the profile parameter q changes significantly with the choice of the intermediate state. Transitions to states $5p^5(^2P_{1/2})\,ns'$ are clearly visible in the spectrum, if intermediate states $5p^5(^2P_{1/2})6p'[1/2]_0$ or $5p^5(^2P_{1/2})6p'[3/2]_2$ with core configuration $^2P_{1/2}$ are selected, while they seem to vanish in the spectrum for an intermediate state $5p^5(^2P_{3/2})6p[1/2]_0$, belonging to core configuration $^2P_{3/2}$. The shape of the $5p^5(^2P_{1/2})\,nd'$-resonances changes, for an intermediate state belonging to the core configuration $^2P_{3/2}$, from a symmetric window-type lineprofile, *i.e.* profile parameter q close to zero, to an strongly asymmetric Beutler-Fano profile with large parameter q for intermediate states of core configuration $^2P_{1/2}$. If third-harmonic generation *via* autoionizing states, *not* involving any resonant coupling to intermediate states, is used to monitor the autoionization spectrum with regard to the spectral line shape, both the $5p^5(^2P_{1/2})\,ns'$- as well as the $5p^5(^2P_{1/2})\,nd'$-resonances are detected. Our data agree with theoretical predictions from calculations based on the configuration interaction Pauli-Fock approximation including core polarization.

We acknowledge support from the European Union, RTN contract No. HPRN-CT-1999-000129, the Deutsche Forschungsgemeinschaft (DFG) as well as the German-Israeli Foundation (GIF), contract No. I-644-118.5/1999. IDP acknowledges support from the DFG through grant No. 436RUS17/1/02. The authors like to thank K. Bergmann and H. Hotop, University of Kaiserslautern as well as V.L. Sukhorukov, Rostov State University for valuable discussion and comments on the manuscript.

References

1. H. Beutler, Z. Phys. **93**, 177 (1935); J. Berkowitz, *Photoabsorption, Photoionization and Photoelectron Spectroscopy* (New York, Academic, 1979); K.D. Bonin, T.J. McIlrath, K. Yoshino, J. Opt. B **2**, 1275 (1985); W. Ernst, T.P. Softley, R.N. Zare, Phys. Rev. A **37**, 4172 (1988); J.Z. Wu, S.B. Whitfield, C.D. Caldwell, M.O. Krause, P. van der Meulen, A. Fahlman, Phys. Rev. A **42**, 1350 (1990); M. Spieweck, M. Drescher, F. Gierschner, R. Irrgang, U. Heinzmann, Phys. Rev. A **58**, 1589 (1998); A. Kortyna, M.R. Darrach, P.T. Howe, A. Chutjian, J. Opt. B **17**, 1934 (2000); U. Hollenstein, H. Palm, F. Merkt, Rev. Sci. Instr. **71**, 4023 (2000)
2. K. Maeda, K. Ueda, K. Ito, J. Phys. B **26**, 1541 (1993)
3. J. Ganz, M. Raab, H. Hotop, J. Geiger, Phys. Rev. Lett. **53**, 1547 (1984)
4. P.R. Blazewicz, J.A.D. Stockdale, J.C. Miller, T. Efthimiopoulos, C. Fotakis, Phys. Rev. A **35**, 1092 (1987); J.L. Dehmer, S.T. Pratt, P.M. Dehmer, Phys. Rev. A **36**, 4494 (1987); S.M. Koekhoven, W.J. Buma, C.A. Lange, Phys. Rev. A **49**, 3322 (1994); S.M. Koekhoven, W.J. Buma, C.A. Lange, Phys. Rev. A **51**, 1097 (1995); M. Gisselbrecht, A. Marquette, M. Meyer, J. Phys. B **31**, L977 (1998)
5. R.F. Stebbings, F.B. Dunning, R.D. Rundel, *Atomic Physics*, edited by G. zu Putlitz, E.W. Weber, A. Winnacker (New York, Plenum, 1975), Vol. 4, p. 713; J.P. Grandin, X. Husson, J. Phys. B **14**, 433 (1981); A. Wada, Y. Adachi, C. Hirose, J. Phys. Chem. **90**, 6645 (1986); L. Wang, R.D. Knight, Phys. Rev. A **34**, 3902 (1986); H. Hotop, D. Klar, S. Schohl, *Resonance Ionization Spectroscopy*, Inst. Phys. Conf. Ser., edited by C.M. Miller, J.E. Parks (Bristol, Inst. Phys. Publishing, 1992), Vol. 128, p. 45; D. Klar, K. Harth, J. Ganz, T. Kraft, M.W. Ruf, H. Hotop, V. Tsemekhman, K. Tsemekhman, M.Y. Amusia, Z. Phys. D **23**, 101 (1992); D. Klar, K. Ueda, J. Ganz, K. Harth, W. Bussert, S. Baier, J.M. Weber, M.W. Ruf, H. Hotop, J. Phys. B **27**, 4897 (1994); J. Landais, M. Huet, H. Kucal, T. Dohnalik, J. Phys. B **28**, 2395 (1995); A. Muehlpfort, U. Even, J. Chem. Phys. **103**, 4427 (1995); R. Kau, D. Klar, S. Schohl, S. Baier, H. Hotop, Z. Phys. D **36**, 23 (1996); S. Schohl, D. Klar, N.A. Cherepkov, I.D. Petrov, K. Ueda, S. Baier, R. Kau, H. Hotop, J. Phys. **30**, 609 (1997); J. Bömmels, J.M. Weber, A. Gopalan, N. Herschbach, E. Leber, A. Schramm, K. Ueda, M.W. Ruf, H. Hotop, J. Phys. B **32**, 2399 (1999); J.M. Weber, K.

Ueda, D. Klar, J. Kreil, M.W. Ruf, H. Hotop, J. Phys. B **32**, 2381 (1999); M. Aslam, R. Ali, A. Nadeem, S.A. Bhatti, M.A. Baig, Opt. Commun. **172**, 37 (1999); D. Klar, M. Aslam, A. Baig, K. Ueda, M.W. Ruf, H. Hotop, J. Phys. B **34**, 1549 (2001)
6. J.C. Miller, R.N. Compton, Phys. Rev. A **25**, 2056 (1982)
7. R. Kau, I.D. Petrov, V.L. Sukhorukov, H. Hotop, Z. Phys. D **39**, 267 (1997)
8. R. Wallenstein, Laser Opt. Elektr. **3**, 29 (1982)
9. J.P. Marangos, J. Mod. Opt. **45**, 471 (1998)
10. M. Protopapas, C.H. Keitel, P.L. Knight, Rep. Progr. Phys. **60**, 389 (1997)
11. *Nonlinear Optics of Autoionizing Resonances*, edited by N. Bloembergen (North Holland, 1977); *Quantum Electronics and Electro-Optics*, edited by P.L. Knight (Wiley, New York, 1983); R.R. Freeman, G.C. Bjorkland, N.P. Economou, P.F. Liao, J.E. Bjorkholm, Appl. Phys. **33**, 739 (1978); G.C. Bjorkland, J.E. Bjorkholm, R.R. Freeman, P.F. Liao, Appl. Phys. **31**, 330 (1977); J.A. Armstrong, J.J. Wynne, Phys. Rev. Lett. **33**, 1183 (1974); R.T. Hudgon, P.P. Sorokin, J.J. Wynne, Phys. Rev. Lett. **32**, 343 (1974)
12. P.L. Knight, M.A. Lauder, B.J. Dalton, Phys. Rep. **190**, 1 (1990)
13. U. Fano, Phys. Rev. **124**, 1866 (1961)
14. H. Beutler, Z. Phys. **86**, 495 (1933); H. Beutler, Z. Phys. **93**, 177 (1935)
15. B.W. Shore, Phys. Rev. **171**, 43 (1968)
16. N.V. Vitanov, T. Halfmann, B.W. Shore, K. Bergmann, Ann. Rev. Phys. Chem. **52**, 763 (2001)
17. E. Arimondo, Prog. Opt. **35**, 259 (1996)
18. T. Halfmann, K. Böhmer, L.P. Yatsenko, A. Horsmans, K. Bergmann, Eur. Phys. J. D **17**, 113 (2001)
19. K. Böhmer, T. Halfmann, L.P. Yatsenko, D. Charalambidis, K. Bergmann, Phys. Rev. A, **66** 013406 (2002)
20. I.D. Petrov, V.L. Sukhorukov, H. Hotop, J. Phys. B **32**, 973 (1999)
21. R. Kau, I.D. Petrov, V.L. Sukhorukov, H. Hotop, Z. Phys. D **39**, 267 (1997)
22. V.L. Sukhorukov, B.M. Lagutin, I.D. Petrov, H. Schmoranzer, A. Ehresmann, K.H. Schartner, J. Phys. B **27**, 241 (1994)
23. V.L. Sukhorukov, V.F. Demekhin, V.A. Yavna, A.I. Dudenko, V.V. Timoshevskaya, Opt. Spec. **55**, 229 (1983)
24. K. Schulz, M. Domke, R. Püttner, A. Gutierrez, G. Kaindl, G. Miecznik, C.H. Greene, Phys. Rev. A **54**, 3095 (1996)
25. Ch.E. Moore, *Atomic Energy Levels* (US Gov. Printing Office, Washington, DC, 1971)
26. S.L. Sorensen, T. Åberg, J. Tulkki, E. Rachlew-Källne, G. Sundström, M. Kirm, Phys. Rev. A **50**, 1218 (1994)
27. I.D. Petrov, V.L. Sukhorukov, H. Hotop, J. Phys. B **35**, 323 (2002)